Background free CARS imaging by phase sensitive heterodyne CARS

M. Jurna, J.P. Korterik, C. Otto*, J.L. Herek, and H.L. Offerhaus

*Optical Sciences group, *BioPhysical Engineering group, MESA+ Institute for Nanotechnology, Faculty of Science and Technology (TNW), University of Twente, the Netherlands*

m.jurna@tnw.utwente.nl

Abstract: In this article we show that heterodyne CARS, based on a controlled and stable phase-preserving chain, can be used to measure amplitude and phase information of molecular vibration modes. The technique is validated by a comparison of the imaginary part of the heterodyne CARS spectrum to the spontaneous Raman spectrum of polyethylene. The detection of the phase allows for rejection of the non-resonant background from the data. The resulting improvement of the signal to noise ratio is shown by measurements on a sample containing lipid.

OCIS codes: (190.4410) Nonlinear optics, parametric processes; (300.6230) Spectroscopy, coherent anti-Stokes Raman scattering; (300.6310) Spectroscopy, heterodyne.

References and links

1. X. Nan, E. Potma, and X. S. Xie, "Nonperturbabtive chemical imaging of organelle transport in living cells with CARS microscopy," Biophys. J. **91**, 728–735 (2006).
2. T. B. Huff and J. X. Cheng, "In vivo coherent anti-Stokes Raman scattering imaging of sciatic nerve tissue," J. Microsc. **225**, 175–182 (2007).
3. T. Hellerer, C. Axäng, C. Brackmann, P. Hillertz, M. Pilon, and A. Enejder, "Monitoring of lipid storage in Caenorhabditis elegans using coherent anti-Stokes Raman scattering (CARS) microscopy," PNAS **104**, 14658–14663 (2007).
4. M. Jurna, J. P. Korterik, H. L. Offerhaus, and C. Otto, "Noncritical phase-matched lithium triborate optical parametric oscillator for high resolution coherent anti-Stokes Raman scattering spectroscopy and microscopy," Appl. Phys. Lett. **89**, 251116 (2006).
5. C. L. Evans, E. O. Potma, M. Puoris'haag, D. Cote, C. P. Lin, and X. S. Xie, "Chemical imaging of tissue in vivo with video-rate coherent anti-Stokes Raman scattering microscopy," Proc. Natl. Acad. Sci. USA **102**, 16807–16812 (2005).
6. J. X. Cheng, A. Volkmer, and X. S. Xie, "Theoretical and experimental characterization of coherent anti-Stokes Raman scattering microscopy," J. Opt. Soc. Am. B **19**, 1363–1375 (2002).
7. E. O. Potma, C. L. Evans, and X. S. Xie, "Heterodyne coherent anti-Stokes Raman scattering (CARS) imaging," Opt. Lett. **31**, 241–243 (2006).
8. S. A. Akhmanov, A. F. Bunkin, S. G. Ivanov, and N. I. Koroteev, "Polarization active Raman spectroscopy and coherent Raman ellipsometry," Sov.Phys. JETP **47**, 667 (1978).
9. A. Volkmer, J. X. Cheng, and X. S. Xie, "Vibrational Imaging with High Sensitivity via Epidetected Coherent Anti-Stokes Raman Scattering Microscopy," Phys. Rev. Lett. **87**, 023901 (2001).
10. F. Ganikhanov, C. L. Evans, B. G. Saar, and X. S. Xie, "High-sensitivity vibrational imaging with frequency modulation coherent anti-Stokes Raman scattering (FM CARS) microscopy," Opt. Lett. **31**, 1872–1874 (2006).
11. Y. S. Yoo, D. H. Lee, and H. Cho, "Differential two-signal picosecond-pulse coherent anti-Stokes Raman scattering imaging microscopy by using a dual-mode optical parametric oscillator," Opt. Lett. **32**, 3254–3256 (2007).
12. A. Volkmer, L. D. Book, and X. S. Xie, "Time-resolved coherent anti-Stokes Raman scattering microscopy: Imaging based on Raman free induction decay," Appl. Phys. Lett. **80**, 1505 (2002).
13. W. P. de Boeij, H. S. Kanger, G. W. Lucassen, C. Otto, and J. Greve, "Waveguide CARS Spectroscopy: A New Method for Background Suppression, Using Dielectric Layers as a Model," Appl. Spectrosc. **47**, 723-730 (1993).

#97810 - $15.00 USD Received 23 Jun 2008; revised 24 Jul 2008; accepted 24 Jul 2008; published 22 Sep 2008

14. V. V. Krishnamachari and E. O. Potma, "Focus-engineered coherent anti-Stokes Raman scattering: A numerical investigation," J. Opt. Soc. Am. A **24**, 1138-1147 (2007).
15. M. Jurna, J. P. Korterik, C. Otto, and H. L. Offerhaus, "Shot noise limited heterodyne detection of CARS signals," Opt. Express. **15**, 15207–15213 (2007).
16. M. Jurna, E. Büttner, J. P. Korterik, C. Otto, I. Rimke, and H. L. Offerhaus , "Shot noise limited heterodyne detection of CARS signals," Proc. SPIE **6860**, 68600R (2008).

1. Introduction

In the last decade Coherent Anti-Stokes Raman Scattering (CARS) microscopy has greatly advanced chemical selective in-vivo imaging on biological tissue [1, 2, 3]. Narrowband CARS provides high resolution detection of molecular transitions [4] and images can be obtained at video rate [5]. The chemical selectivity of CARS microscopy relies on the Raman activity of molecules [6] which gives the CARS signal a unique spectroscopic signature. Nevertheless, CARS vibrational spectra differ from Raman spectra. The frequency dependence of the Raman active vibrational modes can be described by the Lorenzian resonances in the spectrum of the non-linear susceptibility $\chi_R^3(\omega)$:

$$\chi_R^{(3)}(\omega) \propto \sum_{\Omega_k} \left(\frac{a_k}{\Omega_k - \omega - i\Gamma_k} \right), \tag{1}$$

where $\omega = \omega_{pump} - \omega_{Stokes}$, Ω_k is the vibrational resonance of mode k with strength a_k and Γ_k is the full width half maximum of the vibrational band. Both CARS and Raman spectra depend on $\chi_R^{(3)}(\omega)$, but in a different way. The Raman spectrum has only vibration resonant contributions and can be expressed as:

$$I_{Raman}(\omega) \propto Im\chi_R^{(3)}(\omega). \tag{2}$$

The CARS spectrum has vibrational resonant and also contributions, which are not resonant with a vibrational frequency. The non-resonant susceptibility $\chi_{NR}^{(3)}$ is independent of frequency and introduces an offset in the real part of the resonant susceptibility. The CARS spectrum can be described as:

$$I_{CARS}(\omega) \propto \left| \chi_R^{(3)}(\omega) + \chi_{NR}^{(3)} \right|^2. \tag{3}$$

This shows that the Raman and CARS spectra are related to each other, but a direct comparison can only be achieved if both the CARS spectral amplitude and phase are measured. The imaginary part of the CARS amplitude can be compared to the Raman spectrum (Eq. 2). To obtain the CARS intensity the CARS amplitude should be squared. Interferometric detection [7] provides amplitude and phase information and enables CARS imaging without the background (due to e.g. water) of the non-resonant susceptibility. Interferometric detection also provides interferometric amplification. In this paper we focus on those situations where the detection is limited by the non-resonant background rather than the detector noise; we threat only the rejection of the background.

Several methods have been explored to remove the non-resonant background in narrowband CARS, for example PCARS (Polarization CARS) [8] makes use of the different polarization properties of the resonant and non-resonant CARS signal. The non-resonant background can be rejected by placing an analyzer before the detector to select only the resonant contribution. However, when the polarization difference between the resonant and non-resonant signal is small, a large part of the resonant signal is rejected. Another established technique is epi-CARS [9], where the CARS signal is detected in the backward direction. This technique does not offer discrimination between resonant and non-resonant CARS signal directly but between large and small objects in the focal volume. Small resonant objects give rise to a CARS signal in both

#97810 - $15.00 USD Received 23 Jun 2008; revised 24 Jul 2008; accepted 24 Jul 2008; published 22 Sep 2008

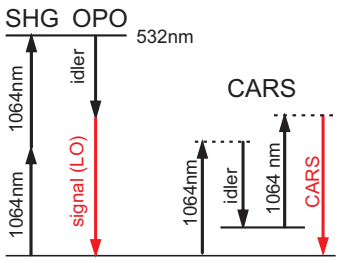

Fig. 1. Energy diagram showing the optical chain for the phase-preserved generation of the wavelengths for the CARS process and Local Oscillator.

the forward and backward direction, where as the surrounding bulk medium causes only non-resonant CARS signal in the forward direction. A recently developed technique is FMCARS (Frequency Modulated CARS) [10], where discrimination between resonant and non-resonant signal is based on modulation of the input frequency for the generation of the CARS signal. Detection at the modulation frequency provides an image that can be compared to the spontaneous Raman image, given some assumptions for the lineshape. FMCARS can also be used in the spectral domain by measuring two discrete wavelengths [11], rather then the modulated integrated signal. Other techniques include time-resolved CARS [12] and spatial phase control CARS [13, 14].

In interferometric CARS [7] the signal is mixed with a reference signal so that amplitude and phase can be detected directly and background free images can be obtained without loss of signal throughout the vibrational spectrum. We have recorded the spectral phase and used it to isolate the imaginary part of the heterodyne CARS spectrum, which can be directly compared to the spontaneous Raman spectrum. The signals are in very good agreement with each other. Subsequently, we demonstrate the use of the phase to obtain background free images.

2. Interferometric detection

Interferometric detection mixes a reference field, the so-called Local Oscillator (LO) field, with the generated CARS field at the anti-Stokes (AS) frequency. The total intensity on the detector can be written as

$$I_{detector} = I_{LO} + I_{AS} + 2\sqrt{I_{LO}I_{AS}}\left\{\left[\chi_{NR}^{(3)} + Re(\chi_R^{(3)})\right] cos\phi + \left[Im(\chi_R^{(3)})\right] sin\phi\right\}, \qquad (4)$$

where ϕ is the phase difference between the total CARS field and the LO field. This is also the phase difference between the (real) non-resonant and the resonant part. For homodyne interferometric detection, a well-controlled and stable LO is required to interfere with the generated CARS field. This LO must be phase- and wavelength-locked to the generated CARS signal. It has been shown previously that the LO can be created in bulk media [7], or using a cascaded phase-preserving chain [15]. Figure 1 shows the energy diagram of the phase-preserving chain. The laser source (1064nm) is partially frequency doubled to 532nm. The 532nm beam synchronously pumps an Optical Parametric Oscillator (OPO), creating a signal and idler wavelength. The CARS signal is generated with the idler from the OPO (Stokes) and the fundamental 1064nm (pump and probe). The signal from the OPO is phase- and wavelength-locked to the generated CARS signal and can therefor be used as the LO.

3. Setup

The setup is based on a Coherent Paladin Nd:YAG laser and an APE Levante Emerald OPO, which provides a well-controlled and stable LO [16]. The power of the signal (LO) of the OPO

#97810 - $15.00 USD Received 23 Jun 2008; revised 24 Jul 2008; accepted 24 Jul 2008; published 22 Sep 2008

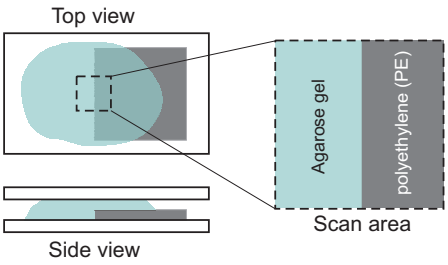

Fig. 2. Schematic of sample used for spectroscopic measurement of amplitude and phase.

is attenuated to a level within the range for shot noise limited detection [15] (few nW) and is combined with the fundamental (1064nm) and the idler (both tens of mW). At this low level, the signal of the OPO does not contribute to the CARS process between fundamental and idler. The three beams are scanned over the sample by galvano mirrors (Olympus FluoView 300, IX71) and focused by a water objective (C.A.R.S., Olympus) lens into the sample. The generated CARS signal and the LO are collected by a collimation lens. The fundamental (ω_{pump}) and idler (ω_{Stokes}) are filtered by two 825-150-2p bandpass filters (Chroma) and the signal is detected by a PMT. To obtain *heterodyne* interferometric detection the CARS frequency is phase shifted by an acousto-optical modulator (AOM) in the 1064nm branch. By detecting the laser repetition rate and using a voltage controlled oscillator (VCO), an external frequency of 50kHz is added to the detected laser repetition rate and applied to the AOM. This 50kHz shift on the 1064nm is translated to a 100kHz shift at the CARS wavelength (twice the external shift due to two photons at 1064nm in the CARS process). The detected intensity on the PMT is fed to a lock-in amplifier set to detect at the 100kHz, the maximum for our lock-in amplifier (Stanford Research SR530). Higher modulation frequencies can be used with a different lock-in amplifier.

4. Verification of phase detection

We first present a spectroscopic measurement of the phase over several overlapping vibrational resonances. The lock-in amplifier is set to 1ms integration time and we use a scanning speed of 5000 pixels/sec over 256x100 pixels. From the lock-in amplifier we obtain both the amplitude and phase for every pixel. The sample, shown schematically in Fig. 2, comprises two adjacent areas. One side consists of agarose gel, which contributes mainly to the non-resonant signal. The other side contains also polyethylene (PE), which gives mostly resonant signal. Scanning the sample reveals a phase step between the non-resonant and resonant sides of the sample. The height of the phase step depends on the spectral position with respect to the vibrational resonance of PE. Due to the small scan area, there is no phase difference caused by the curvature of the field of view, as was verified by measurements on a sample containing only resonant material. The measured amplitude and phase are shown in Fig. 3(a). While tuning the OPO through the high frequency vibrational spectrum of PE, several measurements are recorded and averaged for each region in the sample. The averages are corrected for intensity variations of the input wavelengths. The phase is determined as the difference in phase between the non-resonant and the resonant side of the image. To show that the phase data is in agreement with the amplitude data, the complex dataset, containing both the phase and amplitude information, is fitted to four vibrational levels of PE shown in the CARS spectrum, modeled as Lorenzians bands Eq. (1), with a real offset for the non-resonant background. The fit results in the solid curves for the amplitude and phase as shown in Fig. 3(a), indicating that the measured phase and the spectral amplitude are directly related, as predicted. The phase has an additional offset

#97810 - $15.00 USD Received 23 Jun 2008; revised 24 Jul 2008; accepted 24 Jul 2008; published 22 Sep 2008

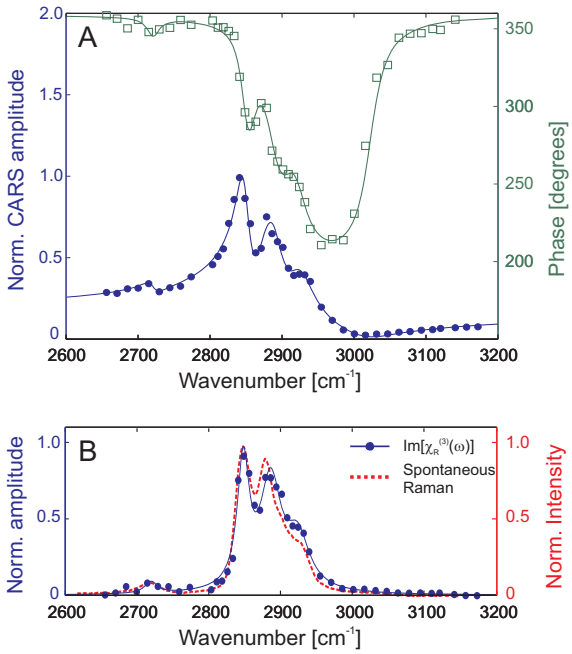

Fig. 3. (a) The CARS amplitude spectrum of the resonant PE (blue circles) and the associated phase of the spectrum (green squares). The symbols are data and the solid curves are fits based on multiple Lorenzian bands as in Eq. (1). (b) The red dotted line is the spontaneous Raman spectrum of PE and in the blue the $\mathrm{Im}\chi_R^{(3)}(\omega)$ of the data in panel A is shown.

of 8 degrees due to the refractive index difference between PE and agarose gel. The graph shows the phase difference between the driving field (difference frequency between pump and Stokes) and the motion of the dipoles in the sample. When the driving frequency is low (left) the response is dominated by the non-resonant response (no phase difference). As the first resonance ($2700\mathrm{cm}^{-1}$) is approached, the phase of the resonant response lags but since this response is weak the phase does not rise to a full difference of π. Subsequent stronger resonances pull the phase much further down. Above the resonances the non-resonant response starts to dominate again, returning the phase difference to zero.

A direct comparison to the spontaneous Raman spectrum of PE can now be made. Figure 3(b) shows the comparison, in blue the imaginary part of the complex dataset and the fit of the CARS measurement are shown and the red dotted line shows the spontaneous Raman spectrum. Very good agreement between the fit and the Raman data indicates that the setup is capable of accurate phase detection.

5. Background rejection

To demonstrate the capability of heterodyne CARS detection for background free imaging, a sample consisting of lipids suspended in agarose gel is scanned. Figure 4 shows the CARS intensity signal generated by the idler and 1064nm. The images consist of 152x152pixels. Figure 4(a) is scanned at 5000pixels/sec and measured directly, Figs. 4(b),(c) are scanned at 600pixels/sec and show the signal after the lock-in amplifier, with an integration time of 3ms/pixel. We have selected a cross section (Fig. 4(e)) at a position (indicated by the green line) where

#97810 - $15.00 USD Received 23 Jun 2008; revised 24 Jul 2008; accepted 24 Jul 2008; published 22 Sep 2008

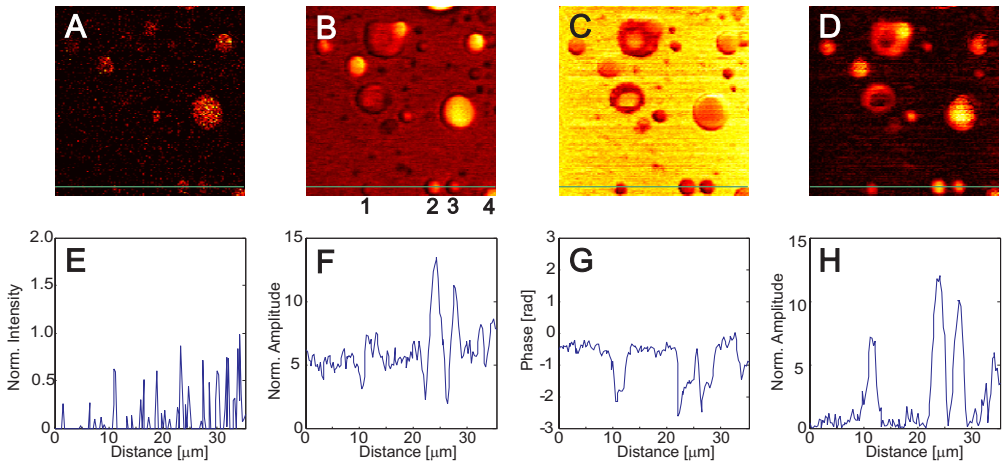

Fig. 4. The sample (35x35μm) contains lipid suspended in agarose gel imaged at 2845 cm^{-1}. (a) Forward intensity CARS image obtained with 1064nm (pump and probe) and idler (Stokes). (b) Amplitude image obtained with heterodyne CARS. (c) Phase image obtained with heterodyne CARS. (d) Im$\chi_R^{(3)}$, the non-resonant free image of the sample. (e-h) Cross sections of the image above at the thin line at the bottom.

the lipid can hardly be seen for figure 4(a). In contrast, using heterodyne CARS, Fig. 4(b),(c) are obtained, which show the amplitude and the related phase of the image respectively. The amplitude image shows several large lipid regions and some smaller ones. The cross section (Fig. 4(f),(g)) intersects 4 of the lipid regions, as numbered in panel 4(b). The smallest lipid region (number 1) has only a signal to noise ratio of 1.5 due to the strong non-resonant signal of the agarose gel. Analyzing the phase image shows that this first region causes a clear phase step compared to the non-resonant signal, which has a flat phase profile across the image. To obtain the background free image, the phase ϕ should be fixed at $1/2\pi$ with respect to the non-resonant phase ($\phi = 0$), see also Eq. (4). By assigning the phase in between the lipid regions (yellow in Fig. 4(c)) to the non-resonant phase, an absolute phase is obtained between the LO and the CARS signal and the resonant part can be extracted. The corresponding image is shown in Fig. 4(d). The first lipid region is now clearly revealed at a signal to noise ratio of $>$15.

6. Conclusions

We have demonstrated that heterodyne CARS, based on a phase preserving chain, can be used to determine amplitude and phase information of the $\chi^{(3)}$ of Raman active vibration modes. A comparison of the imaginary part of the heterodyne signal to the spontaneous Raman spectrum reveals the accuracy of the information. Applying this technique to imaging, we show an order of magnitude improvement in the signal of the amplitude to noise by the suppression of the non-resonant background using the phase.

Acknowledgments

This research is supported by NanoNed, a nanotechnology programme of the Dutch Ministry of Economic Affairs and partly financed by the Stichting voor Fundamenteel Onderzoek der Materie (FOM), which is financially supported by the Nederlandse Organisatie voor Wetenschappelijk Onderzoek (NWO). We also acknowledge Coherent Inc. for the use of the Paladin

laser and APE Berlin for the collaboration and use of a Levante Emerald OPO. Futhermore we would like to thank Ir. L. Hartsuiker (BPE) for her help with the acquisition of the Raman spectra.

#97810 - $15.00 USD Received 23 Jun 2008; revised 24 Jul 2008; accepted 24 Jul 2008; published 22 Sep 2008